Temperature dependence of the dielectric function and the interband critical points of CdSe

S. Logothetidis,* M. Cardona, P. Lautenschlager, and M. Garriga
Max-Planck-Institut für Festkörperforschung, Heisenbergstrasse 1, D-7000 Stuttgart 80, Federal Republic of Germany
(Received 14 March 1986)

The real and imaginary parts of the ordinary and extraordinary dielectric functions of CdSe have been investigated with a scanning rotating analyzer ellipsometer. Strong edge excitons and structure in the 4—5-eV region are observed. With the use of the second derivative versus frequency of these dielectric functions, a critical-point analysis of the observed structures and their temperature dependences has been performed. The obtained results are analyzed in terms of real and imaginary self-energies due to the electron-phonon interaction.

I. INTRODUCTION

Automatic spectral ellipsometry is an excellent technique to investigate the optical response of semiconductors.[1] Assuming a two-phase model of the interface to the outside medium (usually air) a pseudodielectric function $\epsilon(\omega)=\epsilon_1(\omega)+i\epsilon_2(\omega)$ is obtained which can be related to the band structure of the material. A three-phase model makes possible to correct for thin overlayers, such as those produced by oxidation, and thus to extract the true dielectric function of the bulk of the material under study.[1,2] In this manner Ge, Si, and most III-V compounds have been studied at room temperature.[1] On-line digitization of the data permits fast and efficient analysis of the structure observed in the $\epsilon(\omega)$ spectra in terms of standard analytic line shapes for interband critical points.[3] Numerical differentiation of the data facilitates this analysis.

In the past few years we have engaged in a program to investigate systematically the dependence of the critical-point (CP) parameters on temperature[4,5] and other perturbations such as heavy doping with donors or acceptors[6] by means of automatic ellipsometry. In parallel with this experimental work, calculations of the observed shifts and broadenings of critical-point energies have been performed based on realistic band structures and lattice dynamics.[6,7]

While most of this work has been confined to optically isotropic materials (germanium and zinc-blende structures) the usefulness of the experimental method to study anisotropic systems, even optically biaxial ones such as GeS, has also been demonstrated.[8] In this paper we apply the automatic spectral ellipsometry technique to the investigation of the two components of the dielectric function of an optically uniaxial semiconductor, namely CdSe. The measurements were performed for many temperatures between 15 and 550 K. From an analysis of the structures observed in the spectra of the pseudodielectric function the temperature dependence of the energies of the gap excitons and their Lorentzian broadenings are obtained. We also investigate the temperature dependence of the critical-point parameters of additional structures observed in the 4—5.5-eV region.

Cadmium selenide is a prototype of a tetrahedral semiconductor with the hexagonal wurtzite structure.[9] The absorption edge of this material exhibits three excitonic structures which are particularly sharp at low temperature.[10,11] They are usually labeled A (tied to a valence band of Γ_9 symmetry), B (valence band of Γ_7 symmetry), and C (valence band of Γ_7 symmetry). The structures of Γ_7 symmetry (B and C) can be observed for both, the ordinary ($\mathbf{E}\perp\mathbf{c}$) and the extraordinary ($\mathbf{E}\|\mathbf{c}$) polarization directions while that of Γ_9 symmetry (A) can only be observed for $\mathbf{E}\perp\mathbf{c}$. The A and B excitons, which would be degenerate in a zinc-blende-type crystal, are split by the hexagonal crystal field while the C exciton is split from them by the spin-orbit splitting of the top of the valence bands. The complex reflection coefficients around these excitons at very low temperatures are affected by spatial dispersion effects, i.e., by the dependence of the exciton excitation energy on k-vector.[12] Also, the exciton binding energy may become smaller, even vanish, upon approaching the surface, a fact which is often described in terms of an exciton-free (dead) layer.[13] The spatial dispersion effects should be present at very low temperatures only. They should disappear as a result of the exciton broadening for temperatures $T\gtrsim 20$ K in CdSe.[14,15] The dead layer effects will, however, be present even at $T\gtrsim 20$ K. Our calculations show that their influence on the pseudodielectric function is to mix somewhat the real and imaginary parts of the true dielectric function. [This can also be seen from Eq. (1a) of Ref. 1 if one expands the total dielectric constant and keeps only first-order terms in the exciton contribution.]

Ellipsometry is a rather sensitive technique to investigate these effects (as compared, for instance, with normal incidence reflection) as it yields information on both the amplitude and the phase of the reflected beam. Similar results can be obtained, however, from interferometric measurements on thin platelets (see Ref. 14 for CdS). Most of the data available for the A, B, and C excitons of CdSe have been obtained through transmission and reflection measurements in thin platelets.[10,11,16–18] Some data have also been obtained by means of reflectance and electroreflectance measurements on thin samples.[19,20] This work has yielded accurate values for the exciton excitation energies from 1.8 to 300 K.[11,18] The exciton widths

versus temperature, however, have only been partially investigated. The most comprehensive results are given in Ref. 11 for the A exciton. This reference also contains data on the oscillator strength of the A, B, and C excitons.

CdSe is also known to exhibit strong structures in the optical spectra above the edge, in the 4—5.5-eV region.[20,21–24] They correspond to the E_1 and $E_1+\Delta_1$ transitions of the zinc-blende-type materials[20] except for the existence of a strong polarization effect related to the optical anisotropy of wurtzite. For $\mathbf{E}||\mathbf{c}$ only one peak is seen while three are seen for $\mathbf{E}\perp\mathbf{c}$, one of them at nearly the same photon energy as that for $\mathbf{E}||\mathbf{c}$, the other two at lower energies. These structures can be assigned to direct interband transitions[20,25,26] somewhat modified by excitonic interaction.[24,27] By analogy to the zinc-blende case[21] and also as a result of the band calculations[25,26] it is easy to assign the first two peaks observed for $\mathbf{E}\perp\mathbf{c}$ to transitions along the $\Gamma\rightarrow A$ direction between the Γ_5 and the Γ_3 bands. These bands are split by spin-orbit interaction; thus two peaks with a splitting ≈ 0.25 eV are observed. The origin of the additional peak for $\mathbf{E}\perp\mathbf{c}$ and the peak for $\mathbf{E}||\mathbf{c}$ (at ~ 5 eV) lies mainly in transitions along the lateral faces of the Brillouin zone (a hexagonal prism).[25,28]

In this paper we report ellipsometric data for all of these transitions for temperatures between 15 and 550 K. Emphasis is placed on the analysis of critical-point parameters and their temperature dependence. An analysis of this temperature dependence in terms of interaction with phonons of average frequency is performed.

II. EXPERIMENTAL

The measurements were carried out with an automatic spectral ellipsometer of the rotating analyzer type,[29] essentially the same as that described in Ref. 4. The spectra $\epsilon_j(\omega)=\epsilon_{1j}(\omega)+i\epsilon_{2j}(\omega)$ ($j=||$ or $\perp$, meaning parallel or perpendicular to the c axis) of the dielectric function were in general obtained using the two-phase model (ambient and uniaxially anisotropic substrate) of the interface. In this case $\epsilon_j(\omega)$ is sometimes called the "pseudodielectric function" to indicate that no additional corrections for possible surface overlayers or roughness were made. For the edge excitons three-phase models were used so as to account for exciton-free layers. All the spectra were taken at an angle of incidence of 67.5°.

According to the different sharpness of the structures observed in the $\epsilon(\omega)$ spectra, and so as to provide adequate resolution, we used different photon energy spacings for the experimental points. In the region of the A and B edge excitons points spaced by 0.5 meV at 15 K and 1 meV spaced points at higher temperatures were used. A grid of 5 meV was found to be adequate around the energy of the spin-orbit-split C edge exciton, while a 10-meV mesh was used at higher energies for all temperatures. The spectral slit width of our monochromator was ~ 0.6 meV in the region of the edge excitons and 2 meV otherwise. To check for possible jumps in the measured values of $\epsilon(\omega)$ due to changes in the monochromator slits overall spectra were taken periodically with a grid of 10 meV.

For the temperature-dependent measurements a stainless-steel chamber evacuated with a turbomolecular pump was used with two different cold-finger-type sample holders, one for liquid He, the other for liquid N_2 with a heating system built into the cold finger so as to raise the temperature above that of the cryogenic fluid. The sample temperature was determined with two appropriately calibrated iron-constantan thermocouples placed immediately above and below the sample. The temperature stability in the region between 15 and 50 K was typically ± 3 K and about ± 1 K at higher temperatures. The temperature range was limited at low temperatures by the cryostat construction to ~ 15 K and at higher temperatures by the cement (silver paint) which was used to glue the sample to the finger of the cryostat (550 K). During the low-temperature measurements the vacuum was better than 10^{-8} Torr, becoming slightly worse at higher temperatures.

We tried several methods for the preparation of the sample surfaces to be studied. The success of a surface preparation can be checked by the usual criterion[30] that the values of the imaginary part of the dielectric function ϵ_2 be maximized for both principal directions in the ultraviolet region (in standard zinc-blende-type materials around the E_2 gap). Unfortunately, we could not reach the corresponding region for CdSe since it lies in the vacuum uv. We therefore used as a criterion of quality the maximization of ϵ_1 around the E_1 structures observed here (4—5.5 eV, see Fig. 1 of Ref. 30). This criterion was applied to as-grown surfaces parallel to the c axis and subjected to the following treatments. The first includes mechanical lapping and polishing with Syton (Monsanto Chemical Co., St. Louis, MO) in a crystal plane containing the c axis. The distorted layer produced by the

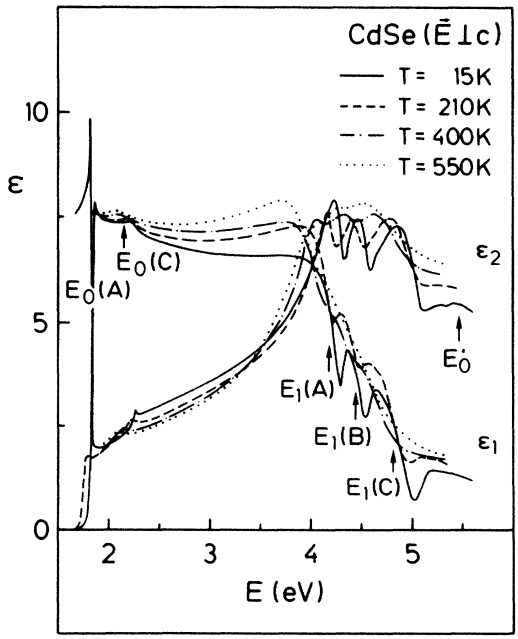

FIG. 1. Real and imaginary parts of the pseudodielectric function of CdSe for light polarized with $\mathbf{E}\perp\mathbf{c}$ at several temperatures between 15 and 550 K.

mechanical polishing is removed by chemical etching with either HF, HNO_3 or NH_4OH, as described in Ref. 30. However, we were not able to maximize ϵ_1 through etching in the E_1 region. Similar negative results were obtained when using a mixture of HNO_3 and HCl. The method used here for surface preparation involved merely the cleaning of a surface of growth with methanol and distilled water while the sample was kept at room temperature inside a windowless cell under the flow of dry N_2. In this case higher values of ϵ_1 than those obtained by etching were found. We did not perform a systematic investigation of possible residual oxide layer since it was not the aim of this paper to obtain quantitatively correct values of the dielectric functions but rather to study the temperature dependence of critical-point parameters. We checked that critical energies and linewidths are not altered by oxide layer corrections with reasonable characteristics. The pseudodielectric functions presented here, however, agree semiquantitatively with those obtained in Ref. 24 by means of normal incidence reflection and transmission techniques.

III. ANALYSIS OF ELLIPSOMETRIC DATA

For the computation of the reflection of obliquely incident polarized light from any anisotropic substrate or film-substrate system, the 4×4 matrix method[2] offers a general unified approach. In our case we assume that the light is incident at an angle θ from the ambient (air) onto a uniaxial anisotropic crystal without any overlayer and with the optic axis c parallel to the interface. $\epsilon_\perp$ and $\epsilon_{||}$ denote the principal components of the dielectric tensor. If the angle between the optic axis c and the plane of incidence α has a value $\alpha\neq0,\pi/2$ we speak of a low-symmetry orientation where the reflection matrix is non-diagonal.[2,31] Such configurations are less preferable for the calculation of the optical constants and we avoided them. If the optic axis takes one of the two high-symmetry orientations $\alpha=0,\pi/2$, the reflection matrix is diagonal and the following relations are obtained for the reflection coefficients for s- and p-polarized light:[2]

$$r_p^1=\frac{\epsilon_\perp^{1/2}\epsilon_{||}^{1/2}\cos\theta-\epsilon_\infty^{1/2}(\epsilon_\perp-\sin^2\theta_0)^{1/2}}{\epsilon_\perp^{1/2}\epsilon_{||}^{1/2}\cos\theta+\epsilon_\infty^{1/2}(\epsilon_\perp-\sin^2\theta_0)^{1/2}}\quad(\alpha=0),\tag{1a}$$

$$r_s^1=\frac{\epsilon_\infty^{1/2}\cos\theta-(\epsilon_\perp-\sin^2\theta_0)^{1/2}}{\epsilon_\infty^{1/2}\cos\theta+(\epsilon_\perp-\sin^2\theta_0)^{1/2}}\quad(\alpha=0),\tag{1b}$$

$$r_p^2=\frac{\epsilon_\perp\cos\theta-\epsilon_\infty^{1/2}(\epsilon_\perp-\sin^2\theta_0)^{1/2}}{\epsilon_\perp\cos\theta+\epsilon_\infty^{1/2}(\epsilon_\perp-\sin^2\theta_0)^{1/2}}\quad(\alpha=\pi/2),\tag{1c}$$

$$r_s^2=\frac{\epsilon_\infty^{1/2}\cos\theta-(\epsilon_{||}-\sin^2\theta_0)^{1/2}}{\epsilon_\infty^{1/2}\cos\theta+(\epsilon_{||}-\sin^2\theta_0)^{1/2}}\quad(\alpha=\pi/2),\tag{1d}$$

where

$$\cos\theta=(1-\sin^2\theta_0/\epsilon_\infty)^{1/2}$$

and ϵ_∞ represents the real dielectric constant of the ambient medium (usually air, $\epsilon_\infty=1$). If an overlayer is present on the sample, the formal (but incorrect) use of Eqs. (1) yields the so-called pseudodielectric function.

Ellipsometry measures the complex ratio ρ between the reflection coefficients r_p and r_s ($\rho=r_p/r_s=\tan\psi e^{i\Delta}$). In the case of a bulk sample with hexagonal symmetry and the optic axis parallel to the reflecting surface, measurements for the two high-symmetry orientations are necessary to calculate the principal components of the dielectric (or pseudodielectric) tensor. At each photon energy ω the four optical parameters ($\epsilon_\perp=\epsilon_{1\perp}+i\epsilon_{2\perp}$, $\epsilon_{||}=\epsilon_{1||}+i\epsilon_{2||}$) can be determined from these two pairs of ellipsometric measurements (ρ_a^m) by means of the following nonlinear relations which connect the measured ellipsometric quantities ρ_a^m to the optical parameters and are obtained from Eqs. (1):

$$\mathrm{Re}(\rho_a^m)=\mathrm{Re}\rho_a^c(\epsilon_{1\perp},\epsilon_{2\perp},\epsilon_{1||},\epsilon_{2||})$$

and

$$\mathrm{Im}(\rho_a^m)=\mathrm{Im}\rho_a^c(\epsilon_{1\perp},\epsilon_{2\perp},\epsilon_{1||},\epsilon_{2||})\ .\tag{2}$$

In Eqs. (2) the index a corresponds to the two orientations in which α takes the values 0 ($a=1$) and $\pi/2$ ($a=2$). The superscripts c and m mean calculated and measured, respectively. The computational procedure consists of applying a method of iteration[2,8,32,33] in order to calculate a vector $A=(\epsilon_{1\perp},\epsilon_{2\perp},\epsilon_{1||},\epsilon_{2||})$ through the minimization of the errorfunction $G(A)$:

$$G(A)=\sum_a^2\{[\mathrm{Re}(\rho_a^m)-\mathrm{Re}(\rho_a^c)]^2+[\mathrm{Im}(\rho_a^m)-\mathrm{Im}(\rho_a^c)]^2\}\ .\tag{3}$$

In the case of the two-phase model, the calculated complex reflectance ratio is $\rho_a^c=r_p^a/r_s^a$ ($a=1,2$), with r_p^a and r_s^a given by Eq. (1).

For the three-phase model (ambient-overlayer-substrate) one has to take into account multiple internal reflections in the film. Addition of the partial waves leads to total complex reflection coefficients, labeled by R, which for the s- and p-polarized components of the light are given by the equations[2]

$$R_\nu^a=\frac{r_{0\nu}+r_\nu^a e^{i2\beta}}{1+r_{0\nu}r_\nu^a e^{i2\beta}}\quad(\nu=p\text{ or }s),\tag{4}$$

where r_ν^a is given in Eq. (1) for ϵ_∞ equal to the dielectric constant of the overlayer and

$$r_{0p}=\frac{\epsilon_\infty^{1/2}\cos\theta_0-(\epsilon_\infty-\sin^2\theta_0)^{1/2}}{\epsilon_\infty^{1/2}\cos\theta_0+(\epsilon_\infty-\sin^2\theta_0)^{1/2}},\qquad r_{0s}=\frac{\cos\theta_0-(\epsilon_\infty-\sin^2\theta_0)^{1/2}}{\cos\theta_0+(\epsilon_\infty-\sin^2\theta_0)^{1/2}}\tag{5}$$

are the reflection coefficients of the interface ambient-isotropic overlayer.

In Eq. (4)

$$\beta=\frac{2\pi d}{\lambda}(\epsilon_\infty-\sin^2\theta_0)^{1/2}$$

is the phase shift in traversing the overlayer and d the thickness of this overlayer. Again, the vector $A=(\epsilon_{1\perp},\epsilon_{2\perp},\epsilon_{1||},\epsilon_{2||})$ can be calculated through minimization of $G(A)$ in Eq. (3), with ρ_a^c defined as $\rho_a^c=R_p^a/R_s^a$ and R_ν^a given by Eq. (4), assuming, however, that ϵ_∞ and the thickness d of the overlayer are known.

The experimental reflection amplitude and phase in CdS and CdSe near the sharp edge excitons (A,B) at low temperature ($T < 10$ K) are strongly affected by spatial dispersion and the presence of a "dead layer."[12,13] In the analysis of our experimental data for CdSe, however, we shall not take into account spatial dispersion. We feel this simplification to be justified by the fact that we only reach temperatures down to 15 K and that the resolution limited linewidths of the sharpest structure observed (~ 2 meV) is close to the characteristic energy above which the spatial dispersion effects disappear.[14,15] In order to explain our ellipsometric data, including asymmetries in the real and imaginary parts of the pseudodielectric functions $\epsilon_\perp$ and $\epsilon_{||}$ observed around the $A_{n=1}$ and $B_{n=1}$ exciton at low temperatures (i.e., mixing of the true $\epsilon_\perp$ and $\epsilon_{||}$) we treat them with a three-phase model which includes a homogeneous exciton-free surface layer (dead layer) of thickness d with a real background dielectric constant ϵ_∞ independent of energy.

IV. RESULTS

A. Pseudodielectric function of CdSe and its temperature dependence

The components ϵ_1 and ϵ_2 of the "ordinary" ($\mathbf{E}\perp\mathbf{c}$) pseudodielectric function of CdSe are shown in Fig. 1 at four different temperatures over the whole spectral range of our measurements. Figure 2 shows similar data for the "extraordinary" ($\mathbf{E}||\mathbf{c}$) components. The A exciton appears only in the $\mathbf{E}\perp\mathbf{c}$ configuration while the first peak for $\mathbf{E}||\mathbf{c}$ is dominated by the B exciton. The E_1 structures exhibit the polarization selection rules reported earlier:[21,24] Three peaks [$E_1(A),(B),(C)$] for $\mathbf{E}\perp\mathbf{c}$ and only one, close to $E_1(C)$, for $\mathbf{E}||\mathbf{c}$. All structures shift to lower energies and broaden with increasing temperature. Towards the end of our spectral range one also observes a structure labeled E_0' in correspondence to structures observed for zinc-blende-type materials.[20] As discussed below, however, the origin of this structure is not clear.

B. Edge excitons

We have plotted in Fig. 3 the ordinary pseudodielectric function of CdSe obtained for photon energies below 2 eV at several temperatures. This energy region covers the range of the A and B excitons. Similar data for the C excitons can be seen in Figs. 1 and 2.

We note in the spectra of ϵ_2 a transformation from Lorentzian-type peaks to step-function-like edges with increasing temperature. Such transformation is expected from Elliott's theory.[34]

The data of Fig. 3 are shown as dashed-dotted lines in Fig. 4 in an expanded energy scale. Figure 5 displays similar data as the curves of the dashed-dotted $\mathbf{E}||\mathbf{c}$ configuration. In Figs. 4 we note considerable deviations from the expected Lorentzian shapes: the maximum and minimum of ϵ_1 are too low, while ϵ_2 is asymmetric, broader towards lower energies. These deviations are easily removed by using a three-phase model with an exciton-free "dead layer" of thickness d and dielectric constant ϵ_∞. The effects of changing d and ϵ_∞ are illustrated in Figs. 4 and 5, respectively. The most symmetric line shapes are obtained for $d = 85$ Å and $\epsilon_\infty = 8$, the latter number being close to what one expects if one removes the exciton dispersion from the data of Figs. 4 and 5.

The inclusion of the dead layer has, however, an unpleasant effect. It introduces slightly negative values of ϵ_2

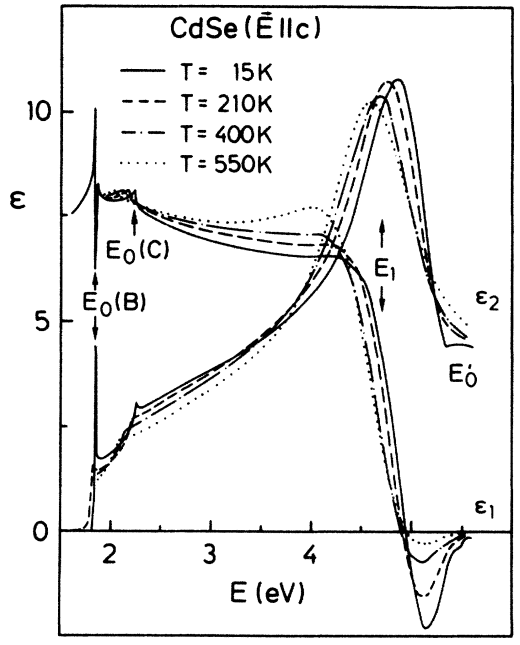

FIG. 2. Real and imaginary parts of the dielectric function of CdSe for light polarized with $\mathbf{E}||\mathbf{c}$ at several temperatures between 15 and 550 K.

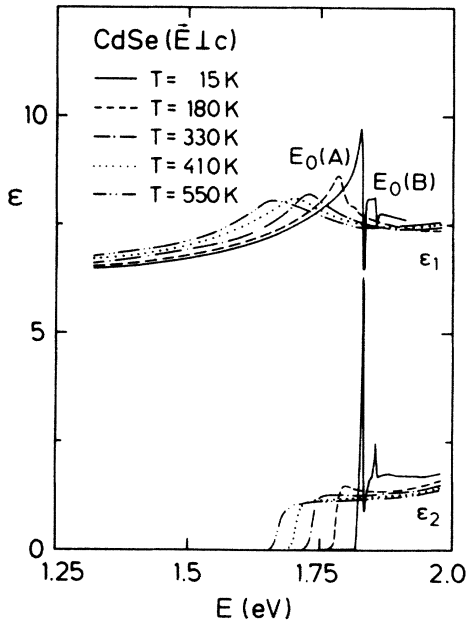

FIG. 3. Real and imaginary parts of the dielectric function of CdSe for light polarized with $\mathbf{E}\perp\mathbf{c}$ in the $E_0(A)$ and $E_0(B)$ exciton region and below at several temperatures between 15 and 550 K.

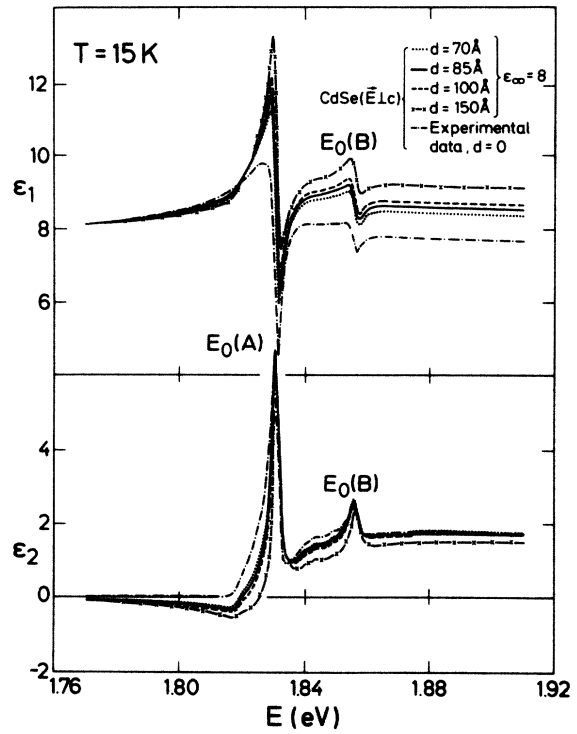

FIG. 4. Real (ϵ_1) and imaginary (ϵ_2) parts of the dielectric function of CdSe for light polarized with $\mathbf{E}\perp\mathbf{c}$ in the $E_0(A)$ and $E_0(B)$ exciton region at 15 K with corrections for an exciton-free (dead) layer of thickness d and background dielectric constant ϵ_∞, for a fixed value of $\epsilon_\infty = 8$ and various values of d.

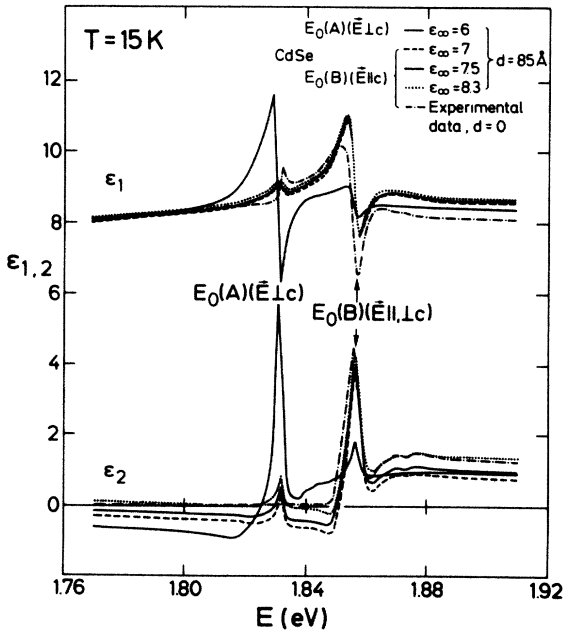

FIG. 5. Real (ϵ_1) and imaginary (ϵ_2) parts of the dielectric function of CdSe for light polarized with $\mathbf{E}||\mathbf{c}$ and $\perp\mathbf{c}$ in the $E_0(A)$ and $E_0(B)$ exciton region, as corrected for an exciton-free (dead) layer of thickness d and background dielectric function ϵ_∞, for a fixed value, of $d = 85$ Å and various values of ϵ_∞.

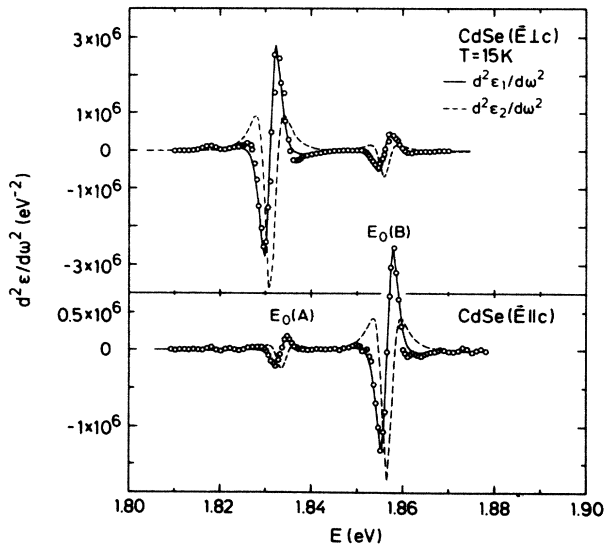

FIG. 6. Second derivatives of the real (solid line) and imaginary (dashed line) part of the dielectric function of CdSe (corrected for exciton-free layer) as a function of energy in the $E_0(A)$ and $E_0(B)$ exciton region at 15 K, for the two principal polarizations studied. The experimental points are given only for $d^2\epsilon_1/d\omega^2$.

below the A frequency. In view of the fact that in this region rotating analyzer ellipsometry yields only rather inaccurate values of ϵ_2, we believe that the problem just mentioned may simply be due to the inaccuracy of the method and thus that ϵ_2 should be taken equal to zero below A.

We also note that the strengths expected for the A and B excitons in the ordinary and extraordinary configurations ($A = 0$ in the $\mathbf{E}||\mathbf{c}$ case, B small, $\sim\frac{1}{3}A$ in the $\mathbf{E}\perp\mathbf{c}$ case[11,35]), are approximately fulfilled. The weak A peak observed in Fig. 5 for $\mathbf{E}||\mathbf{c}$ is probably due to residual depolarization by the cryostat windows or to slight misorientation of the sample.

We show in Figure 6 the fits to the second derivative spectra of the dielectric functions of the A and B excitons obtained with the three-phase model. The fits were performed with Lorentzian line shapes. A dead layer thickness $d \approx 100$ Å with $\epsilon_\infty = 8$ gives the best fits. We note that at 15 K the Lorentzian broadening parameters (half width, half maximum) are 2.1 ± 0.2 meV for the A exciton, 2.6 ± 0.1 meV for the B exciton, and 10 ± 1 meV for the C exciton. The oscillator strength per CdSe molecule found for the A exciton for $\mathbf{E}\perp\mathbf{c}$ is 2.4×10^{-3}. It compares well with that given in Ref. 11 (2.25×10^{-3}).

V. CRITICAL-POINT PARAMETERS AND THEIR TEMPERATURE DEPENDENCE

A. Edge excitons

The edge exciton line shapes measured at low temperatures and their derivatives can simply be fitted with Lorentzian functions (Fig. 6). As the temperature increases, however, the ϵ_2 line shapes transform into a step

function (Fig. 3). We have, therefore, chosen to fit the A, B, and C excitons throughout the whole temperature range with the expression

$$\epsilon=\frac{A_1}{\omega-E_0+i\Gamma}-A_2e^{i\Phi}\ln(\omega-E_0+i\Gamma)+A_3\,, \tag{6}$$

whereby for the C excitons A_1 turns out to be negligible. The imaginary part of the logarithm in Eq. (6) is a broadened step function.

We plot in Fig. 7 the variation of the critical point energies E_0 with temperature obtained for the A, B, and C excitons by the procedure just mentioned. The data have been fitted with two different functions. One of them (dashed lines) is the phenomenological expression

$$E(T)=E(0)-\frac{\alpha T^2}{T+\beta} \tag{7}$$

proposed by Varshni.[36] The other (solid lines), based on the theory of the temperature shift of the gap produced by electron-phonon interaction,[7,37] is

$$E(T)=E_B-a_B(2n_B+1)\,,\qquad n_B=\left[\exp\left[\frac{\Theta}{T}\right]-1\right]^{-1}\,, \tag{8}$$

where Θ is a temperature which corresponds to an average phonon frequency. The parameters of the fits with Eqs. (7) and (8) are listed in Table I. The fits with the two equations are of the same quality, so that the lines in Fig. 7 coincide, except for low temperatures, where the difference in energy is still smaller than 4 meV.

We note in Table I that α, which represents the linear shift in E_0 at high temperatures. has values similar to those found for the direct band edge of other tetrahedral semiconductors[18] ($\alpha=4\times10^{-4}$ eV K^{-1} for Ge, 5.8×10^{-4} eV K^{-1} for GaAs). It is not fully clear which of the two Eqs. (7) and (8) better fits the experimental points. However, at low temperatures, Eq. (8) seems to fit somewhat better, as may be expected in view of the microscopic basis of this equation. The obtained average phonon temperatures Θ, around 150 K, are reasonable in view of the fact that the maximum phonon frequency corresponds to 300 K.[18]

The linewidths of critical points versus temperature are usually fitted with an expression similar to Eq. (8). This expression includes broadening through phonon absorption and emission. For the lowest gap or the lowest edge exciton A, however, only phonon absorption should contribute to the broadening. The same thing would hold for B if polar optical phonons near Γ are the main broadening agent. We should thus use for the A and B excitons

$$\Gamma(T)=\Gamma_1+\Gamma_0n_B\,, \tag{9}$$

where Γ_1 represents the broadening due to elastic scattering plus instrumental broadening. For the C exciton we replace n_B in Eq. (9) with $2n_B+1$ since now both phonon absorption and emission processes can take place. Two such fits have been performed in Fig. 8, one over the whole temperature range and the other restricted to the 15–250 K region. The parameters of the fit are listed in

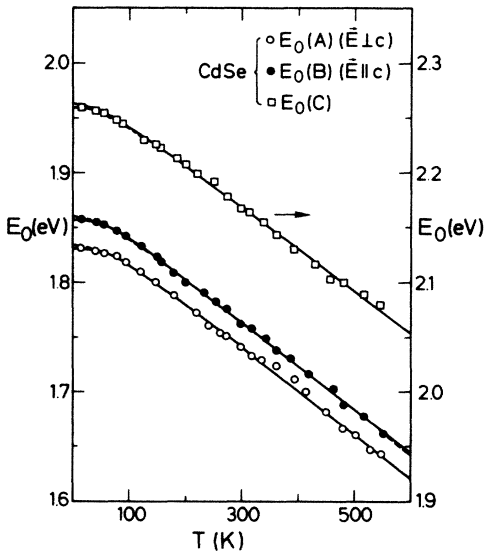

FIG. 7. Temperature dependence of the edge exciton excitation energies of CdSe for E⊥c and E||c. Two fits to the experimental points were performed: one with Eq. (8) (solid line) and the other with Eq. (7) (dashed line below 100 K and above 500 K). The difference between these two fits is unperceptible except for $T<100$ K and for $T>500$ K, where the difference is nevertheless less than 4 meV. Typical error bars for the experimental points are given in Table III.

TABLE I. Values of $E(0)$, α, and β parameters obtained by fitting the excitation energies of the edge excitons versus temperature with Eq. (7) and of E_B, a_B, and Θ parameters obtained from a fit with Eq. (8). The 95% confidence limits are given in parentheses.

	$E(0)$ (eV)	α (10^{-4} eV K^{-1})	β (K)	E_B (eV)	a_B (meV)	Θ (K)
			E⊥c polarization			
$E_0(A)$	1.834 (3)	4.24 (20)	118 (40)	1.866 (5)	36 (5)	179 (40)
$E_0(C)$	2.263 (4)	3.96 (20)	81 (35)	2.286 (5)	27 (8)	142 (40)
$E_1(A)$	4.316 (2)[a]	8.47 (40)[a]	174 (40)[a]	4.386 (10)[a]	77 (10)[a]	206 (30)[a]
$E_1(B)$	4.567 (8)	8.92 (70)	265 (100)	4.67 (3)	112 (40)	290 (80)
$E_1(C)$	5.063 (10)	8.24 (20)	40 (20)	5.092 (9)	35 (10)	84 (40)
			E∥c polarization			
$E_0(B)$	1.860 (2)	4.17 (10)	93 (20)	1.887 (4)	31 (6)	152 (25)
$E_1(C)$	5.131 (10)	8.89 (40)	39 (20)	5.163 (10)	39 (10)	89 (40)

[a]Between 15 and 420 K.

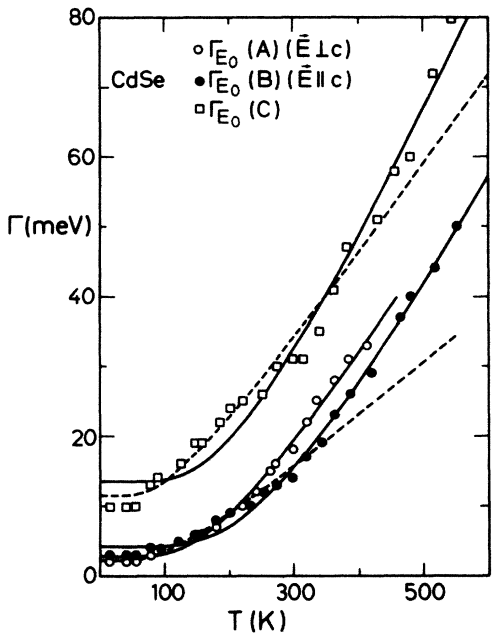

FIG. 8. Temperature dependence of the broadening parameters of the edge excitons of CdSe. The solid and dashed lines represent the best fits with Eq. (9) with Θ variable and with $\Theta=300$ K, respectively.

Table II. We note that the Θ obtained for the fit of the whole temperature range is much higher than the highest phonon temperature. Moreover, these fits are rather poor in the 100–300 K interval. We feel that this is an artifact related to the transition from the Lorentzian to the step function line shape. The fits to the points in the 15–250 K interval (dashed lines) were performed using a fixed $\Theta=300$ K, corresponding to the uppermost LO phonons at Γ. These phonons are expected to be mainly responsible for the broadening of the A and B excitons.[38]

In Table III we compare the excitation energies obtained by us for the A, B, and C edge excitons at 80 K and room temperature with other recent data.[16,24,39] More data for these energies can be found in Ref. 18. In comparing them to ours, we should keep in mind that the energies of Ref. 16 correspond to the reflectance maxima and not to the true excitation energies which should be shifted up from the reflectance maximum by $\lesssim\Gamma$. Although without a line shape analysis of the data of Ref. 16 it is not possible to make a precise comparison with our results, it seems that the excitation energies given in the latter are somewhat higher than the former (~ 5 meV). A similar conclusion is reached when comparing our results at 15 K with those of Ref. 3. We cannot find, at present, the source of this discrepancy which could be due, e.g., to different degrees of impurities in the samples (sulfur?) or to differential strains produced by our sample holder.

B. Interband critical points

From fits to the data of Figs. 1 and 2 we have also determined the parameters of the $E_1(A)$, $E_1(B)$, and $E_1(C)$ critical points. We obtained rather good fits with the function

$$\epsilon = C - A\ln(\omega - E_1 + i\Gamma)e^{i\Phi}, \tag{10}$$

which corresponds to a general two-dimensional critical point.[40] Examples of these fits are shown in Fig. 9 for the second derivative of $\epsilon(\omega)$. The critical-point energies so obtained are shown in Fig. 10, and the corresponding broadening parameters versus temperature in Fig. 11. The general trend is similar to that observed for the E_0 excitons although the energy shift is nearly twice as large (the broadenings, however, are comparable). The parameters of the fits to the data of Figs. 10 and 11 with Eqs. (7), (8), and

TABLE II. Values of the parameters involved in the temperature dependence of the Lorentzian broadening of the CP's observed in the dielectric function of CdSe. The broadening is represented for $E_0(A)$ and $E_0(B)$ transitions by Eq. (9) and by either Eq. (11) or the linear expression $\Gamma(T)=\Gamma_{L+\gamma}T$ for all other CP's. The 95% confidence limits are given in parentheses.

	Γ_1 (meV)	Γ_0 (meV)	Θ (K)	Γ_L (meV)	γ (10^{-4} eV K^{-1})
			E⊥c polarization		
$E_0(A)$	2.7 (6)	81 (20)	530 (85)		
	2.3 (3)[a]	23 (1)[a]	300[a]		
$E_0(C)$	−50 (20)	64 (25)	613 (160)		
	−9 (2)[a]	20 (2)[a]	300[a]		
$E_1(A)$	−11 (10)[b]	50 (20)[b]	458 (110)[b]		
	19 (3)[c]	16 (1)[c]	206[c]		
$E_1(B)$	42 (3)	9 (4)	129 (60)		
$E_1(C)$	64 (8)	18 (7)	120 (70)	71 (3)	2.82 (14)
			E∥c polarization		
$E_0(B)$	4 (1)	139 (25)	775 (86)		
E_1				215 (7)[b]	4.34 (34)[b]

[a]Between 15 and 250 K with fixed parameter $\Theta=300$ K.
[b]Between 15 and 400 K.
[c]Between 15 and 250 K and the parameter Θ has been fixed to have the same value as for the energy shift of the $E_1(A)$ critical point.

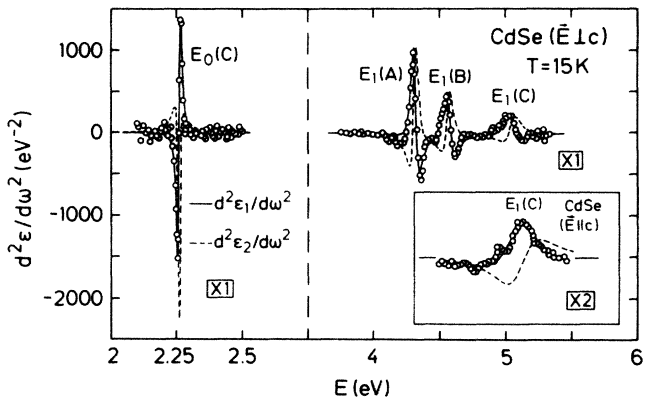

FIG. 9. Fits to the second derivatives of the real (solid line) and imaginary (dashed line) parts of the pseudodielectric function of CdSe as functions of the energy at 15 K in the $E_0(C)$ and E_1 regions. The dots represent experimental points for $d^2\epsilon_1/d\omega^2$. The energy scale around $E_0(C)$ has been enlarged by a factor of 2. The inset shows the $E_1(C)$ CP's for light polarized with $\mathbf{E}||\mathbf{c}$; the vertical scale has been expanded by a factor of 2.

$$\Gamma(T)=\Gamma_1+\Gamma_0(2n_B+1) \tag{11}$$

are given in Tables I and II. We have given for $E_1(C)$ in Table II also the results of a linear fit

$$\Gamma(T)=\Gamma_L+\gamma T, \tag{12}$$

which, in this case, represents the data rather well. We note that the negative values of Γ_1 in Table II simply result from the fit and may have no physical meaning. It may, in the case of $E_1(A)$, be taken equal to zero within error.

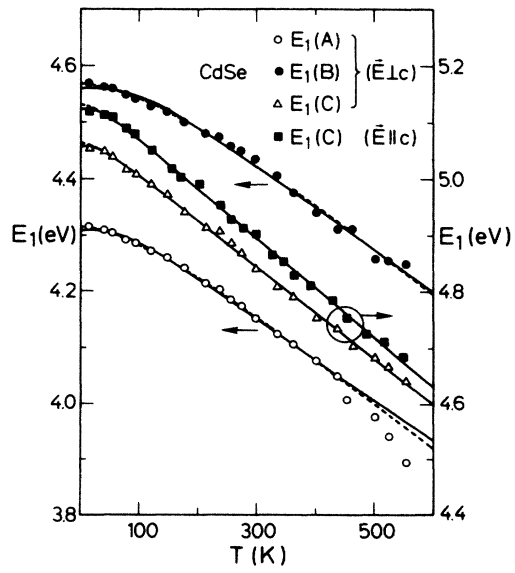

FIG. 10. Temperature dependence of the E_1 critical-point energies of CdSe for $\mathbf{E}\perp\mathbf{c}$ and $\mathbf{E}||\mathbf{c}$. The lines have the same meaning as in Fig. 7.

TABLE III. Excitation energies (in eV) of the $E_0(A)$, $E_0(B)$, and $E_0(C)$ excitons observed in CdSe by us and other authors with **E** perpendicular and parallel to the c axis at several temperatures. Also, data for the E_1 and E_0' critical points. The 95% confidence limits for our data are given in parentheses.

	80 K exciton reflectance Ref. 16	80 K Our data	90 K reflectivity Ref. 41	109 K ϵ_2 peak Ref. 24	295 K Our data	293 K exciton reflectance Ref. 16	295 K Ref. 24
			E⊥c polarization				
$E_0(A)$ (Γ_{9v}-Γ_{7c})	1.8134 (3)	1.8230 (2)			1.741 (3)	1.735	
$E_0(C)$ (Γ_{7v}-Γ_{7c})	2.242 (1)	2.248 (1)			2.167 (9)	2.160 (2)	
$E_1(A)$ (Γ_{5v}-Γ_{3c})		4.292 (2)	4.18	4.25	4.152 (6)		4.12
$E_1(B)$ (Γ_{5v}-Γ_{3c})		4.548 (5)	4.50	4.50	4.438 (20)		4.30
$E_1(C)$ (U_{4v}-U_{3c})		5.015 (16)	4.87	4.92	4.838 (42)		4.79
E_0' (H_{3v}-H_{3c})			5.6	5.66[a]			5.55[a]
			E∥c polarization				
$E_0(B)$ (Γ_{7v}-Γ_{7c})	1.8390 (5)	1.8460 (3)			1.762 (3)	1.755 (2)	
E_1 (U_{3v}-U_{3c})		5.089 (20)	4.95	4.92	4.903 (31)		4.79

[a]Unpolarized light.

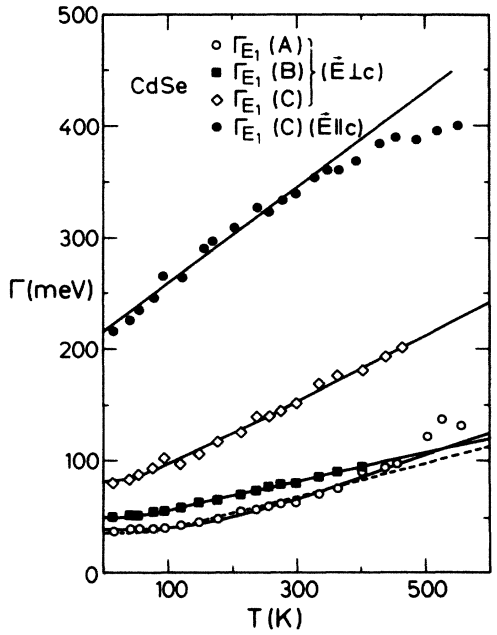

FIG. 11. Temperature dependence of the broadening parameters of the E_1 CP's of CdSe. The solid lines for the E_1 transitions for light polarized with $\mathbf{E}\perp\mathbf{c}$ represent the best fits with Eq. (11) and that with $\mathbf{E}\parallel\mathbf{c}$ the best linear fit. The dashed line for the $E_1(A)$ transition represents the best fit with Eq. (11), where the parameters Θ is fixed ($\Theta=206$ K).

VI. DISCUSSION

A. Edge excitons

In the analysis of the edge excitons we have neglected spatial dispersion effects. This should be justified if the linewidths are much larger than a critical linewidth γ_0 given by[14,15] (in atomic units)

$$\gamma_0=\left[\frac{4\pi f\alpha}{V_M}\right]^{1/2}, \tag{13}$$

where f is the oscillator strength per molecule, V_M is the volume per molecule, and α is related to the exciton translational mass M through

$$\alpha=\frac{E_0}{2Mc^2}, \tag{14}$$

where c is the speed of light in vacuum. For $M\simeq 0.4$ (Ref. 18) we find $\gamma_0\simeq 0.5$ meV with the value of $f=2.4\times10^{-3}$ obtained from our fits. Since all the observed linewidths $\Gamma\gtrsim 2$ meV we believe that neglecting spatial dispersion is justified. We should point out, however, that the observed linewidths are largely instrumental since our total resolution is $\simeq 1$ meV.

In order to fit our data for the A and B excitons to Lorentzian expressions we have found it necessary to use a three-phase model with an exciton dead layer whose thickness was ≈ 100 Å. We note that the exciton radius can be estimated from

$$a_{\rm ex}=\frac{1}{2E_b\epsilon_0}, \tag{15}$$

where $E_b\simeq 15$ meV, is the exciton binding energy and $\epsilon_0\simeq 10$ the static dielectric constant (in atomic units). From Eq. (15) we find $a_{\rm ex}\simeq 50$ Å. Hence the thickness of the dead layer amounts to $2a_{\rm ex}$, a rather reasonable value.

The oscillator strength per molecule obtained for the A exciton is 2.4×10^{-3}. It can also be estimated theoretically with the expression[38,3]

$$f=\frac{4(2E_b)^3\epsilon_0^3V_M}{E_0\pi}\,|\hat{\mathbf{e}}\cdot\mathbf{p}|^2, \tag{16}$$

where $\hat{\mathbf{e}}$ is the direction of the electric field and $\mathbf{p}$ the transition matrix element. For the A exciton with $\hat{\mathbf{e}}\perp\mathbf{c}$ we take by analogy with zinc-blende structure:

$$|\hat{\mathbf{e}}\cdot\mathbf{p}|^2=\frac{1}{2}\left[\frac{2\pi}{(4V_M)^{1/3}}\right]^2\simeq 0.15, \tag{17}$$

with $E_b=15$ meV and $\epsilon_0=10$. Equation (16) thus yields $f_A=1.5\times10^{-3}$ somewhat smaller than the experimental value (2.4×10^{-3}).

The temperature dependence of the broadening of the A and B excitons is determined by LO-phonon absorption (Fröhlich interaction).[38] The constant broadening Γ_1 of Eq. (9) and Table II is largely instrumental, partially also caused by impurity and boundary scattering. The temperature-dependent term is given by the coefficient Γ_0 of Table II. As mentioned in Sec. IV B the most reliable value of Γ_0 for the A exciton is 23 meV (Table II). This value can be compared with those calculated in Ref. 38 for CdS ($\Gamma_0=43$ meV) and CdTe ($\Gamma_0=10$ meV): It falls halfway inbetween, as expected. The mechanism just discussed also contributes to the broadening of the C exciton, but in this case deformation potential scattering to the A and B bands, with phonon emission and absorption, is dominant.[41]

The negative value of $\Gamma_1(C)$ given in Table II can have no physical value. In fact, it is possible to rewrite $\Gamma(C)$ as (in meV)

$$\Gamma(C)=-9+20(2n_B+1) \tag{18a}$$

$$=11(2n_B+1)+18n_B\ . \tag{18b}$$

The first term in Eq. (18b) represents scattering to the A,B bands while the second one gives the interband scattering through LO-phonon absorption and, as expected, is similar to the corresponding term for the A band. The coefficient of the interband term for the A band. The coefficient of the interband term (11 meV) is rather similar to that found for GaAs (10 meV),[41] as expected since the deformation potential mechanism depends little on the ionicity of the material. Actually, a slight decrease in deformation potential may be compensated by the increase in the Frölich interaction with increasing ionicity.

B. Structures in the E_1 region

The original assignment of these structures was made by analogy to the E_1 and $E_1+\Delta_1$ peaks of the zinc-blende-type materials.[21] One of the $\langle 111\rangle$ directions (we call it [111]) of the Brillouin zone of zinc-blende can be mapped onto the c axis of wurtzite (Γ-Δ-A) (Ref. 25), while the other three directions map, in principle, into ar-

bitrary directions which can be pushed by symmetry requirements down to the basal plane (Γ-Σ-M direction) or to the top (A-R-L) of the wurtzite Brillouin zone. The E_1 and $E_1+\Delta_1$ transitions along the [111] direction of zinc-blende will preserved their spin-orbit splitting Δ_1 when mapped along the Γ-Δ-A direction of wurtzite. Band calculations have corroborated these original assumptions.[25,26] The equivalent of the E_1 transitions of zinc-blende along [111] are expected to be allowed only for $\mathbf{E}\perp\mathbf{c}$ and spin-orbit split by an amount

$$\frac{2}{3}\left[E_c-\frac{E_A+E_B}{2}\right]=0.28\ \text{eV}\ . \tag{19}$$

This splitting should not vary much with temperature. These requirements are fulfilled by the $E_1(A)$ and $E_1(B)$ structures observed in Fig. 1 for $\mathbf{E}\perp\mathbf{c}$ and not in Fig. 2 ($\mathbf{E}\|\mathbf{c}$): Their splitting, 0.25 eV, is shown in Fig. 10 to be nearly independent of temperature. Band calculations,[25,26] confirm that the second highest valence band and the second lowest conduction band along Γ-Δ-A which correspond to the E_1 transitions of zinc-blende along [111], are nearly parallel and thus should contribute to optical structure.

The remaining $\langle 111\rangle$ directions lead to unpolarized transitions in zinc-blende. Hence, it is reasonable to attribute to them the $E_1(C)$ peaks of wurtzite (Figs. 1 and 2) which can be seen at nearly the same energy for both polarizations. Band calculations together with calculations of the combined density of states[25] suggests that the main contribution to these transitions comes from the M-U-L line, which joins the M and L points on the side faces of the Brillouin zone. The $U_4\rightarrow U_3$ transitions are mainly polarized for $\mathbf{E}\perp\mathbf{c}$ while $U_3\rightarrow U_3$ are polarized for $\mathbf{E}\|\mathbf{c}$. At the M point, where valence and conduction band are more closely parallel (see Fig. 8 of Ref. 25), the $M_4\rightarrow M_3$ gap is about 0.1 eV less than $M_3\rightarrow M_3$, a fact which would explain why the $E_1(C)$ experimental energy for $\mathbf{E}\perp\mathbf{c}$ is $\approx$0.06 eV less than for $\mathbf{E}\|\mathbf{c}$ (see Table I).

We have already commented on the large shift of the E_1 critical points with temperature. At high temperature the shift is linear, as expected, with a coefficient around -8.5 (in units of 10^{-4} eV K) Fig. 10 and Table I). For Ge the coefficient of the e_1 gaps is around -6 and for Si it is ~ -3.[7] The temperature dependence of the broadenings of the $E_1(A)$, $E_1(B)$, and $E_1(C)$ (Fig. 11, Table II), however, is rather similar to that found for Ge and Si.[4,37] For the zinc-blende-type II-VI compounds (ZnSe, ZnTe, CdTe) the shift coefficients lie around -6 (10^{-4} eV K). Hence we believe that the large temperature coefficients found for the E_1 gaps of CdSe are a property of the wurtzite structure which should also be checked for CdS and analyzed through "first principles" calculations of the type performed in Refs. 7 and 37 for Ge and Si.

The strength factor A of Eq. (10), obtained from the fit to the second derivative spectra, has the dimensionless value 8 for $E_1(C)$ in the $\mathbf{E}\|\mathbf{c}$ configuration, nearly independent of temperature. The three E_1 structures for $\mathbf{E}\perp\mathbf{c}$ have at low temperatures $A\simeq 1.5$ each. This value was found to decrease somewhat with increasing temperature.

The strength of the E_1 and $E_1+\Delta_1$ structures of zinc-blende-type materials can easily be estimated with the simple expression[5,40]

$$A(E_1)\simeq 44\frac{(E_1+\Delta_1/3)}{a_0E_1^2}\simeq\frac{44}{a_0E_1}\ ,$$
$$A(E_1+\Delta_1)\simeq 44\frac{(E_1+2\Delta_1/3)}{a_0(E_1+\Delta_1)^2}\simeq\frac{44}{a_0(E_1+\Delta_1)}\ , \tag{20}$$

where a_0 is the lattice constant in Å and E_1,Δ_1 the gaps and spin-orbit splittings in eV. In the spirit of this approximation one would expect for the E_1 transitions of CdSe for $\mathbf{E}\|\mathbf{c}$

$$A(E_1(C))=\frac{44}{(2V_m)^{1/3}E_1(C)}=1.4\ , \tag{21a}$$

and for $\mathbf{E}\perp\mathbf{c}$:

$$A(E_1(A))=\frac{3}{8}\frac{44}{(2V_M)^{1/3}E_1(A)}=0.6\ ,$$
$$A(E_1(B))=\frac{3}{8}\frac{44}{(2V_M)^{1/3}E_1(B)}=0.6\ , \tag{21b}$$
$$A(E_1(C))=\frac{5}{8}\frac{44}{(2V_M)^{1/3}E_1(C)}=0.9\ .$$

These values of the strength parameter A are all considerably smaller than the experimental ones given above. Although one may attribute this to the extremely crude

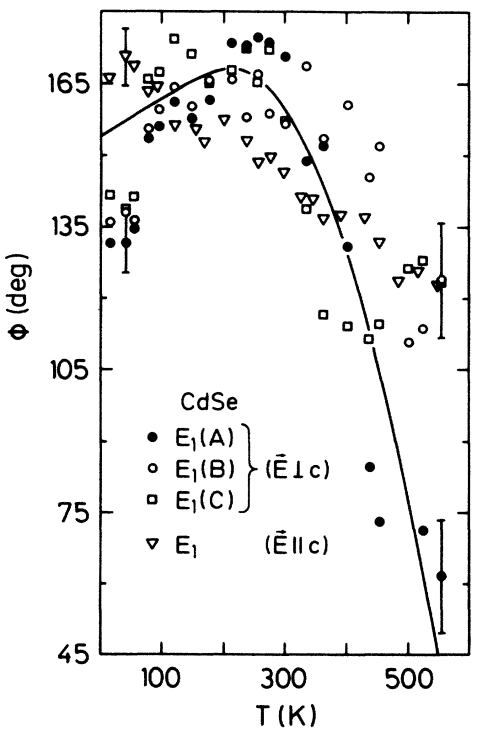

FIG. 12. Temperature dependence of the phase angles obtained by fitting the E_1 critical points with Eq. (10). The solid line, representing the average phase angle, is drawn as a guide to the eye.

model used, discrepancies have also been found for zinc-blende-type materials for which the model should work better.[5] They have been attributed to excitonic enhancement of the oscillator strength.[27,42,43] The excitonic nature of the E_1 transitions is quite apparent in Fig. 1: ϵ_1 exhibits sharp dips *above* the critical energies instead of the symmetric $-\ln|\omega-\omega_0|$ shapes expected for two-dimensional critical points. This result is similar to that found for other II-VI compounds. It can be quantified through the phase angle Φ of the fitting function [Eq. (10)]: $\Phi=0$ would be expected for two-dimensional minima. Instead (Fig. 12) values as large as 165° are found. Except for a small anomalous increase at low temperatures, the values of Φ decrease with increasing temperature and seem to tend to zero at high temperatures, thus signaling a decrease in the excitonic effects. Similarly the strengths of the $E_1(A)$ and $E_1(B)$ structures decrease from ~ 1.5 to ~ 0.6: The latter would agree with the predictions of Eq. (21).[44] Unfortunately the strength of $E_1(C)$ is nearly independent of temperature.

We cannot give a reliable assignment of the E_0' structure which is only seen for $\mathbf{E}\perp\mathbf{c}$ (Fig. 1). According to Ref. 25 it may be related to $M_2\rightarrow M_1$ transitions which have the required polarization.

ACKNOWLEDGMENTS

One of us (M.G.) acknowledges financial support of Caixa de Pensions "la Caixa," Barcelona (Spain). The CdSe samples used were kindly given to use by Mrs. Broser-Warminski, Fritz-Haber-Institut, Berlin. We thank G. Vignale for a critical reading of the manuscript.

*Permanent address: First Laboratory, Solid State Physics Section, Aristotle University of Thessaloniki, Thessaloniki, Greece.

[1]D. E. Aspnes and A. A. Studna, Phys. Rev. B **27**, 985 (1983), and references therein.

[2]See, e.g., R. M. A. Azzam and N. M. Bashara, *Ellipsometry and Polarized Light* (North-Holland, Amsterdam, 1977).

[3]M. Cardona, *Modulation Spectroscopy* (Academic, New York, 1969).

[4]L. Viña, S. Logothetidis, and M. Cardona, Phys. Rev. B **30**, 1979 (1984).

[5]S. Logothetidis, L. Viña, and M. Cardona, Phys. Rev. B **31**, 947 (1985).

[6]L. Viña and M. Cardona, Phys. Rev. B **29**, 6739 (1984).

[7]P. Lautenschlager, P. B. Allen, and M. Cardona, Phys. Rev. B **31**, 2163 (1985).

[8]S. Logothetidis, L. Viña, and M. Cardona, Phys. Rev. B **31**, 2180 (1985).

[9]See, for instance, *Physics and Chemistry of II-VI Semiconducting Compounds,* edited by M. Aven and J. S. Prener (North-Holland, Amsterdam, 1967), Chap. 1.

[10]R. G. Wheeler and J. O. Dimmock. Phys. Rev. **125**, 1805 (1962).

[11]J. Voigt, F. Spiegelberg, and M. Senoner, Phys. Status Solidi B **91**, 189 (1979); S. F. Terekhova, N. A. Onishchenko, O. N. Talenskii, and S. A. Pendur, *ibid.* **131**, 207 (1985).

[12]C. Gourdon and P. Lavallard, Phys. Rev. B **31**, 6654 (1985), and references therein.

[13]J. J. Hopfield and D. G. Thomas, Phys. Rev. **132**, 563 (1963).

[14]M. S. Brodin, N. A. Davydova, and M. I. Strashnikova, Phys. Status Solidi B **70**, 365 (1975).

[15]A. S. Davydov and E. N. Myasnikov, Phys. Status Solidi B **63**, 325 (1974).

[16]V. V. Sobolev, V. I. Donetskikh, and E. F. Zagainov, Fiz. Tekh. Poluprovdn. **12**, 1089 (1978) [Sov. Phys.—Semicond. **12**, 646 (1978)].

[17]R. B. Parsons, W. Wardzynski, and A. D. Yoffe, Proc. R. Soc. London, Ser. A **262**, 120 (1961).

[18]*Landolt-Börnstein Tables,* edited by O. Madelung, M. Schulz, and H. Weiss (Springer, Berlin, 1982), Vols. 17a and 17b.

[19]M. Cardona and G. Harbeke, Phys. Rev. **137**, A1467 (1965).

[20]M. Cardona, K. L. Shaklee, and F. H. Pollak, Phys. Rev. **154**, 696 (1967).

[21]M. Cardona, Phys. Rev. **129**, 1068 (1963); Solid State Commun. **1**, 109 (1963).

[22]R. Ludeke and W. Paul, in *Proceedings of the 7th International Conference on II-VI Semiconducting Compounds, Brown University, 1967,* edited by D. G. Thomas (Benjamin, New York, 1967), p. 123.

[23]I. A. Iliev, M. N. Iliev, and H. Lange, Phys. Status Solidi B **69**, K157 (1975).

[24]H. Lange and I. A. Iliev, Phys. Status Solidi B **84**, 569 (1977).

[25]T. K. Bergstresser and M. L. Cohen, Phys. Rev. **164**, 1069 (1967).

[26]A. Kobayashi, O. F. Sankey, S. M. Volz, and J. D. Dow, Phys. Rev. B **28**, 935 (1983).

[27]S. Antoci and G. F. Nardelli, Phys. Rev. B **6**, 1311 (1972).

[28]R. L. Hengehold and C. R. Fraime, Phys. Rev. **174**, 808 (1968).

[29]D. E. Aspnes, Opt. Commun. **8**, 222 (1973); D. E. Aspnes and A. A. Studna, Appl. Opt. **14**, 220 (1975).

[30]D. E. Aspnes, J. Vac. Sci. Tehnol. **17**, 1057 (1980); Appl. Phys. Lett. **34**, 316 (1981).

[31]T. P. Sosnowski, Opt. Commun. **4**, 408 (1972).

[32]R. Matz and H. Lüth, Appl. Phys. **18**, 123 (1979).

[33]S. Logothetidis, S. Ves, and J. Spyridelis, Phys. Status Solidi B **122**, 613 (1984).

[34]R. J. Elliot, Phys. Rev. **108**, 1384 (1957).

[35]J. L. Birman, in *Excitons,* edited by E. I. Rashba and M. D. Sturge (North-Holland, Amsterdam, 1982), Chap. 2.

[36]K. P. Varshni, Physica (Utrecht) **34**, 149 (1967).

[37]P. Lautenschlager, P. B. Allen, and M. Cardona, Phys. Rev. B **33**, 5501 (1986).

[38]B. Segall, *Proceedings of the International Conference on the Physics of Semiconductors, Moscow, 1968* (Nauka, Leningrad, 1968), p. 425.

[39]R. B. Hall and H. H. Woodbury, J. Appl. Phys. **39**, 5361 (1968).

[40]M. Cardona, in *Atomic Structure and Optical Properties of Solids,* edited by E. Burstein (Academic, New York, 1972), p. 514.
[41]P. Lawaetz, DSc. thesis, Technical University of Denmark, 1978 (unpublished).
[42]W. Hanke and L. Sham, Phys. Rev. B **21**, 4656 (1980).
[43]I. Balslev, Solid State Commun. **52**, 351 (1985).
[44]M. Cardona, J. Appl. Phys. **36**, 2181 (1965).